

Nonlinear effects in optical pumping of a cold and slow atomic beamN. Porfido,^{1,*} N. N. Bezuglov,^{2,3} M. Bruvelis,⁴ G. Shayeganrad,^{1,†} S. Birindelli,^{1,‡} F. Tantussi,^{1,§} I. Guerri,¹ M. Viteau,⁵ A. Fioretti,^{6,7} D. Ciampini,^{1,6,7} M. Allegrini,^{1,6,7} D. Comparat,⁸ E. Arimondo,^{1,6} A. Ekers,⁹ and F. Fuso^{1,6,7}¹*Dipartimento di Fisica Enrico Fermi, Università di Pisa, 56127 Pisa, Italy*²*Faculty of Physics, St. Petersburg State University, 198904 St. Petersburg, Russia*³*Department of Physics, University ITMO, 197101 St. Petersburg, Russia*⁴*Institute of Atomic Physics and Spectroscopy, University of Latvia, LV-1586 Riga, Latvia*⁵*Orsay Physics, TESCAN Orsay, 13710 Fuveau, France*⁶*Istituto Nazionale di Ottica, INO-CNR, 56124 Pisa, Italy*⁷*Consorzio Nazionale Interuniversitario per le Scienze Fisiche della Materia, CNISM, Sezione di Pisa, 56127 Pisa, Italy*⁸*Laboratoire Aimé Cotton, CNRS, Université Paris-Sud, ENS Cachan, 91405 Orsay, France*⁹*Computer, Electrical and Mathematical Sciences and Engineering Division, King Abdullah University of Science and Technology, Thuwal 23955-6900, Kingdom of Saudi Arabia*

(Received 29 June 2015; published 12 October 2015)

By photoionizing hyperfine (HF) levels of the Cs state $6^2P_{3/2}$ in a slow and cold atom beam, we find how their population depends on the excitation laser power. The long time (around 180 μ s) spent by the slow atoms inside the resonant laser beam is large enough to enable exploration of a unique atom-light interaction regime heavily affected by time-dependent optical pumping. We demonstrate that, under such conditions, the onset of nonlinear effects in the population dynamics and optical pumping occurs at excitation laser intensities much smaller than the conventional respective saturation values. The evolution of population within the HF structure is calculated by numerical integration of the multilevel optical Bloch equations. The agreement between numerical results and experiment outcomes is excellent. All main features in the experimental findings are explained by the occurrence of “dark” and “bright” resonances leading to power-dependent branching coefficients.

DOI: [10.1103/PhysRevA.92.043408](https://doi.org/10.1103/PhysRevA.92.043408)

PACS number(s): 32.80.Xx, 37.20.+j, 37.10.-x

I. INTRODUCTION

Optical pumping is known to strongly affect population distributions in atomic energy level systems interacting with resonant light fields (see [1] and references therein for a more complete list of investigations in this area). A number of experimental and theoretical studies have been performed to understand optical pumping in level systems exhibiting hyperfine (HF) and Zeeman structure [2], its dependence on excitation intensity [3], interaction time with the radiation field [4], and the presence of external magnetic fields [5]. Most of those studies have been performed in Doppler-free experiments either in vapor cells [4,6] or in thermal and supersonic atom beams [3,7] (for a review on pioneering experiments and interpretation of optical pumping effects, see, e.g., [8]).

Accurate description of the optical pumping effects requires a precise determination of the atom-light interaction-time regimes that were rather ambiguous in most of earlier studies. For instance, in vapor cells there is no net direction in the motion of atoms, and it is very difficult to accurately define the interaction time [4,9]. Moreover the broad thermal velocity distribution of atoms blurs the average atom-light interaction

time, and collisions often partially, or even fully, cancel the alignment effects which usually result from optical pumping. Experiments employing orthogonally crossed atom and laser beams substantially improve the definition of interaction time and nearly eliminate collision effects, yet they are usually constrained with respect to the attainable atom-light interaction (transit) time to typical values up to a few tens of microseconds, unless laser beams with very large diameters are used.

Here, we study optical pumping by selective resonant excitation of HF transitions in cesium atoms belonging to a slow and cold beam. The low longitudinal velocity of the beam enables exploring the long-interaction-time regime. Furthermore, the excited-state population is analyzed, with negligible perturbation, through photoionization and ion-counting techniques, achieving a sensitivity large enough to explore the investigated effects over a wide range of pumping power.

The combination of laser manipulation of atoms and their photoionization is presently receiving a great deal of attention for several applications; for instance, in the realm of focused ion beam (FIB) technologies, see, e.g., [10–16]. Within that context, this combination can offer an unprecedented degree of control over the dynamical properties of the produced ions. In the present paper, a conceptually similar ability to control the atomic state and to determine its population is used in order to get reliable and reproducible experimental results. Comparing them with numerical simulations, based on a comprehensive model of the atom-light interaction, allows us to point out the nonlinear behavior of optical pumping processes, evident even at relatively weak pumping laser intensity. The large atom-light interaction time accessible in our experiment leads to a very large number of population pumping cycles between both hyperfine levels and Zeeman sublevels observed already in

*Present address: ASML, 5504 DR Veldhoven, Netherlands.

†Present address: Fakultät Physik, Zentrum für Synchrotronstrahlung, Technische Universität Dortmund, 44227 Dortmund, Germany.

‡Present address: Department of Applied Physics, Technische Universiteit Eindhoven, 5612 AJ Eindhoven, Netherlands.

§Present address: Istituto Italiano di Tecnologia, 16136 Genova, Italy.

[17], such that strong nonlinear effects, such as those reported in [18], are observed even in the weak-excitation regime, well below the conventional saturation intensity for a two-level system.

The analysis developed in the present work is based on the treatment developed by some of us in [3] for the optical pumping in a simple two-level open system. That analysis is here extended to real cases by including the complexity of a multilevel system. For our investigation, performed in the limit of long interaction times, a weak excitation by a weak-intensity laser strongly modifies the atomic evolution and finally plays an important role in the interpretation of experimental results. In a regime of weak optical pumping where the slow temporal evolution of the atomic variable determines the measured variables, the standard approach of an analytical solution for the steady state cannot be applied to interpret the results. Instead, the full temporal evolution of the density-matrix equations is examined. For saturation absorption spectroscopy this same approach was applied in Ref. [19] to investigate nonstationary effects and in Ref. [20] to study the role of multilevel systems.

Section II lists the basic issues of the laser-atom interaction with reference to the optical pumping processes in multilevel open systems. Section III describes the experimental setup. Section IV reports the experimental results for the measured variable, i.e., the ion counts produced by the photoionization of the laser-excited atomic state and also determines the absorption line strengths and the laser critical intensity for the onset of the optical pumping leading to modifications in the ion counts. Section V describes the approach adopted for the numerical solution of the time-dependent density-matrix equations. Section VI reports the results of the numerical solution along with a detailed analysis of the experimental findings.

II. BASICS OF OPEN TWO-LEVEL SYSTEMS

A. Pump rate and time scale

Let us start with the simple case of a semiopen two-level system consisting of a ground state g and an excited state e . Interaction of such a system with a laser field of Rabi frequency Ω and detuning δ produces a lifetime $1/\Gamma_g$ of the state g , leading to a broadening Γ_g of the $g \rightarrow e$ transition [21,22],

$$\Gamma_g = \Omega^2 \frac{\Gamma_e}{\Gamma_e^2 + 4\delta^2}. \quad (1)$$

The natural broadening of the transition is equal to the spontaneous emission rate of photons from the e state Γ_e , with $\tau_e = 1/\Gamma_e$ being the natural lifetime. In a partially open system, only a fraction Π (the so-called branching coefficient) of the spontaneous transition processes produce a return of population to state g . The decay to levels other than g defines the population leakage from the (g,e) system, occurring at the rate $(1 - \Pi)\Gamma_g$. When the excitation laser frequency is in resonance with the transition ($\delta = 0$), the time scale of the population depletion from the (g,e) system is [3]

$$\tau_{pump} = \frac{1}{(1 - \Pi)\Gamma_g} = \frac{\Gamma_e}{\Omega^2(1 - \Pi)}. \quad (2)$$

B. Two-level atom in the long-transit-time limit

When the transit time τ_{tr} of atoms through the laser field is longer than the optical pumping time, $\tau_{tr} > \tau_{pump}$, the population of the (g,e) system is depleted. In terms of Rabi frequencies this condition can be rewritten as

$$\Omega > \Omega_{cr} \cong \Omega_{sat} \sqrt{\frac{2\tau_e}{\tau_{tr}(1 - \Pi)}}, \quad \Omega_{sat} = \frac{\Gamma_e}{\sqrt{2}}, \quad (3)$$

where Ω_{sat} is the saturation Rabi frequency [22]. Ω_{cr} is a critical value of the Rabi frequency whose meaning and relevance will be further clarified in Sec. IV B.

Equation (3) implies that $\Omega_{cr} \ll \Omega_{sat}$ if $\tau_{tr} \gg \tau_e$. If this is the case, one can further distinguish three different regimes of optical pumping:

(i) $\Omega < \Omega_{cr}$. No considerable population pumping occurs within the transit time, and there is poor sharing of population between states g and e . The population of state e increases linearly with the laser intensity.

(ii) $\Omega_{cr} < \Omega < \Omega_{sat}$. In this regime, $\tau_{pump} \ll \tau_{tr}$; hence population is lost from the $g-e$ system within a time much shorter than the duration of the interaction between light and atoms. In experiments involving an atom beam crossing the excitation laser beam, the spatial distributions of the populations of the states g and e are strongly modified within a small region near the entrance of atoms into the laser beam, and the populations decrease exponentially with the penetration into the laser beam. We write for the occupations $n_{e,g}(t)$ of those states, $n_{e,g}(t) \sim \exp(-t/\tau_{pump})$; at long interaction times $t \gg \tau_{pump}$ both states are empty. In a configuration where the excited-state population is measured in the whole interaction volume, for instance, through photoionization as in the present experiment, the measured signal J is proportional to the time-integrated occupation of the excited state (see, e.g., Sec. V in [3]), given by

$$\bar{n}_e = \int_{-\infty}^{\infty} dt n_e(t), \quad \bar{n}_e = \frac{\tau_e}{1 - \Pi} \left[1 - \exp\left(-\frac{\tau_{tr}}{\tau_{pump}}\right) \right]. \quad (4)$$

The saturation of \bar{n}_e at the $\tau_e/(1 - \Pi)$ value leads to saturation in the measured signal.

(iii) $\Omega > \Omega_{sat}$. Under such conditions, the rate of laser-induced transitions ($\sim \Omega$) exceeds the spontaneous transition rate Γ_e . The splitting between the laser-dressed states, which is proportional to Ω , exceeds their width $\Gamma_e/2$, and the population is equally shared between the states e and g [22]. The pumping time stabilizes at the value $\tau_{pump} = \tau_{sat} = 2/[\Gamma_e(1 - \Pi)]$ and becomes independent of any further increase of the excitation laser intensity. The \bar{n}_e -averaged occupation of Eq. (4) saturates at the limit

$$\bar{n}_e^{(sat)} = \frac{\tau_e}{1 - \Pi} \left[1 - \exp\left(-\frac{\tau_{tr}}{\tau_{sat}}\right) \right]. \quad (5)$$

Equations (4) and (5) have a straightforward physical interpretation: the number of photons spontaneously emitted on transitions to levels outside the $g-e$ system, $\Gamma_e \bar{n}_e (1 - \Pi)$, is equal to the total loss of ground-state occupation for a single atom during its interaction with the laser field, $[1 - \exp(-\tau_{tr}/\tau_{pump,sat})]$.

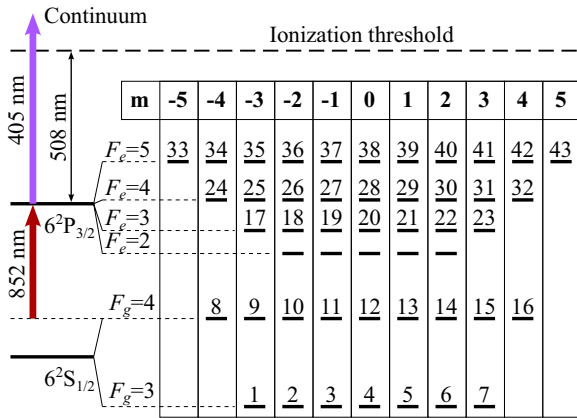


FIG. 1. (Color online) Excitation and photoionization scheme for cesium D_2 line with hyperfine structure and magnetic Zeeman sublevels. Laser excitation occurs from $F_g = 4$. Magnetic Zeeman sublevels are numbered according to Eqs. (13).

C. Dynamic effects in multilevel atoms

In realistic multilevel atoms that exhibit hyperfine and Zeeman sublevels, the dynamics of optical pumping is obviously more complex. Here, we study the population dynamics in Cs $6^2P_{3/2}$ HF sublevels upon excitation by linearly polarized laser light resonant with the D_2 transition. A simplified level scheme, including also the photoionization path accomplished with 405-nm radiation, which brings the electrons to an energy ≈ 0.34 eV above the continuum threshold, is shown in Fig. 1. The whole array of emission and absorption paths involving, for instance, the single selected pair of HF states with $F_g = F_e = 4$, hereafter denoted as T44 transition, is depicted in Fig. 2(a). Due to the selection rules, $m=0 \rightarrow m=0$ transitions are in this case forbidden [23]. The $m_g = 0$ sublevel is thus not involved in optical pumping and behaves as a dark

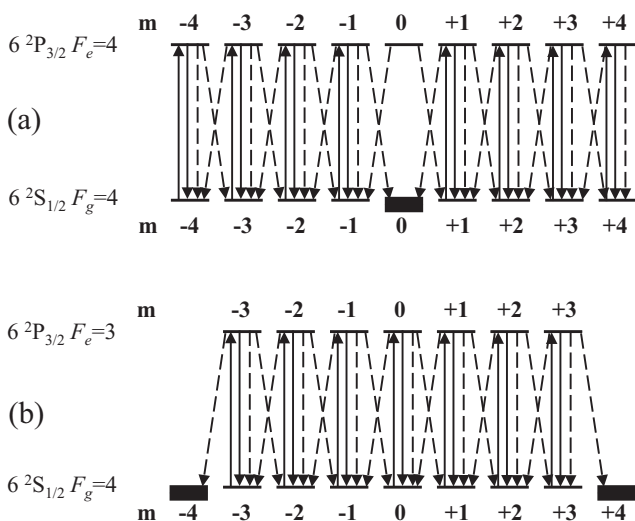


FIG. 2. Zeeman structure for the (a) T44 and (b) T43 transitions upon π polarized excitation. The solid arrows show the absorption and stimulated emission transitions, while the dashed ones depict the spontaneous emission paths. The thick levels denote the population accumulation due to optical pumping.

state [22]. For the transition involving the pair of HF states with $F_g = 4, F_e = 3$, hereafter denoted as T43, the role of the dark states is played by the outermost Zeeman sublevels, $|F_g = 4, m = \pm 4\rangle$ [see Fig. 2(b)].

The dark-state population can survive deep into the laser-atom interaction zone. This can have important consequences especially when the long-interaction-time regime is explored. For instance, even a weak coupling of states induced by a relatively weak laser intensity can be sufficient to retrieve some of the trapped population in the investigated transition. Furthermore, other effects can lead to nonlinear dynamical effects, including those associated with the formation of the so-called bright resonances [24], which will be discussed in Sec. VI B within the context of optical pumping on the T45 transition.

III. EXPERIMENTAL SETUP

The experimental setup is based on an apparatus already used for nanofabrication experiments and discussed in detail elsewhere [25–27]. We combine a slow and cold atom beam produced out of a pyramidal magneto-optical trap (pyramidal MOT) with a photoionization stage used to probe excited-state population. Since the ionization rate is much lower than the involved radiative transition rates, the detection of Cs^+ ions allows for a nonperturbing analysis of excited-state populations. Moreover, in contrast to most saturated absorption spectroscopy experiments [17], we can safely disregard any optical pumping effect due to atom interaction with the probe laser field owing to the relatively weak laser intensity.

A schematic diagram of the apparatus is shown in Fig. 3. The pyramidal MOT [28,29] produces a continuous flow of $(6 \pm 2) \times 10^9$ atoms/s, with an average longitudinal velocity $\langle v \rangle \simeq 12$ m/s and a width of the Maxwellian velocity distribution around 1.5 m/s, FWHM [30]. Two-dimensional transverse

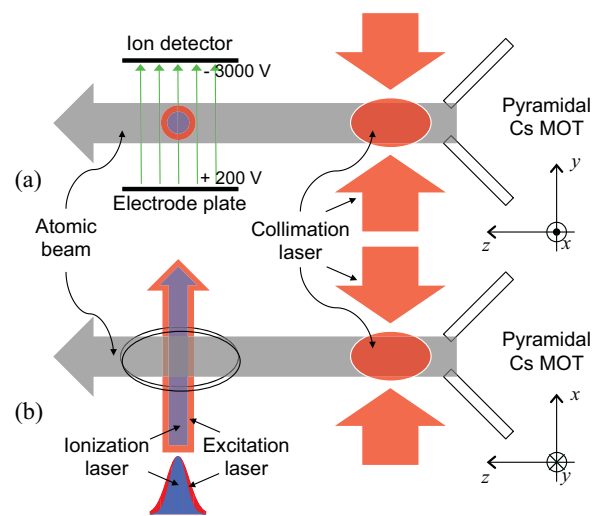


FIG. 3. (Color online) Schematic diagram of the experimental setup: (a) side and (b) top views are reported. The electric field guiding the ions towards the detector is depicted in (a), whereas the spatial distributions of the superposed excitation (pump) and ionization (probe) laser beams are drawn at the bottom of (b). Drawing not to scale.

optical molasses right after the pyramid apex reduces the beam divergence angle to 4 mrad (FWHM).

Downstream from the collimation stage, after a free-flight distance of 30 cm, the atoms enter the interaction region. Here, the atomic beam, with a transverse size around 4 mm (FWHM), is crossed at right angles by two collimated linearly polarized and spatially superposed cw laser beams, the pump laser for resonant excitation of ground-state Cs atoms, and the probe laser for photoionization of the excited atoms. The diameter of the probe beam is smaller than that of the pump beam. This geometrical arrangement ensures that photoionization probes the population in the region of the highest excitation intensity and the atoms excited in the purely linear regime by the wings of the excitation beam profile do not obscure the observation of the nonlinear effects.

An electrode plate (10 mm diameter, placed 35 mm below the ionization zone and biased at +200 V) produces the electric field needed to guide the ions towards the detector (electron multiplier EM226 Thorn-EMI), which is placed 80 mm above the ionization zone and biased at -3000 V. The anode of the detector is connected to a gated counter (Stanford Research Systems SR400), from which the recorded signal is sent to a computer for further analysis. The measured signal is represented by the ion count rate, i.e., the number of ion counts in 1-s gate time. Data uncertainty is obtained by measuring the standard deviation over a large number (typically, several hundreds) gate intervals.

All trapping, collimation, and excitation laser beams are generated by diode lasers operated at 852 nm in the master-slave configuration and delivering a maximum output power of about 100 mW. Master lasers are coupled to grating-ended external optical cavities (Littrow configuration) in order to allow for tuning; the emission frequency is locked to Cs reference cells probed in the Doppler-free configuration. Repumping radiation is provided within the pyramid volume by a distributed Bragg reflector (DBR) laser. The ionizing laser beam (maximum power 10 mW) is generated by a single-mode GaN diode laser (Oxxius) with internally stabilized current and temperature, operating at 405 nm. Both the excitation and ionization laser beams have been checked to have a Gaussian shape well described by $\exp(-z^2/w_z^2)\exp(-y^2/w_y^2)$ functions, with $w_z^{exc} = (1.1 \pm 0.1)$ mm and $w_y^{exc} = (1.5 \pm 0.1)$ mm, $w_z^{ion} = (0.69 \pm 0.01)$ mm and $w_y^{ion} = (1.65 \pm 0.03)$ mm, respectively. The corresponding transit times of atoms through the laser beams are accordingly $\tau_{tr,exc} = 2w_z^{exc}/\langle v \rangle \simeq 180 \mu\text{s}$ and $\tau_{tr,ion} = 2w_z^{ion}/\langle v \rangle \simeq 100 \mu\text{s}$.

IV. EXPERIMENTAL RESULTS AND CONVENTIONAL INTERPRETATION

The measured ion count rate is shown in Fig. 4 as a function of the excitation laser power for the excitation frequency locked on a selected HF transition: $F_g=4 \rightarrow F_e=5$ (T45), $F_g=4 \rightarrow F_e=4$ (T44), and $F_g=4 \rightarrow F_e=3$ (T43). Apart from the obvious observation that the ion signal in all cases grows with increasing excitation laser power, a couple of differences are evident: (i) the count rate for the T45 transition grows significantly faster with laser power than it does in the other two cases, and (ii) a very small increase in the count rate is observed for T43 and T44 at pump power W_{exc} between ~ 0.02

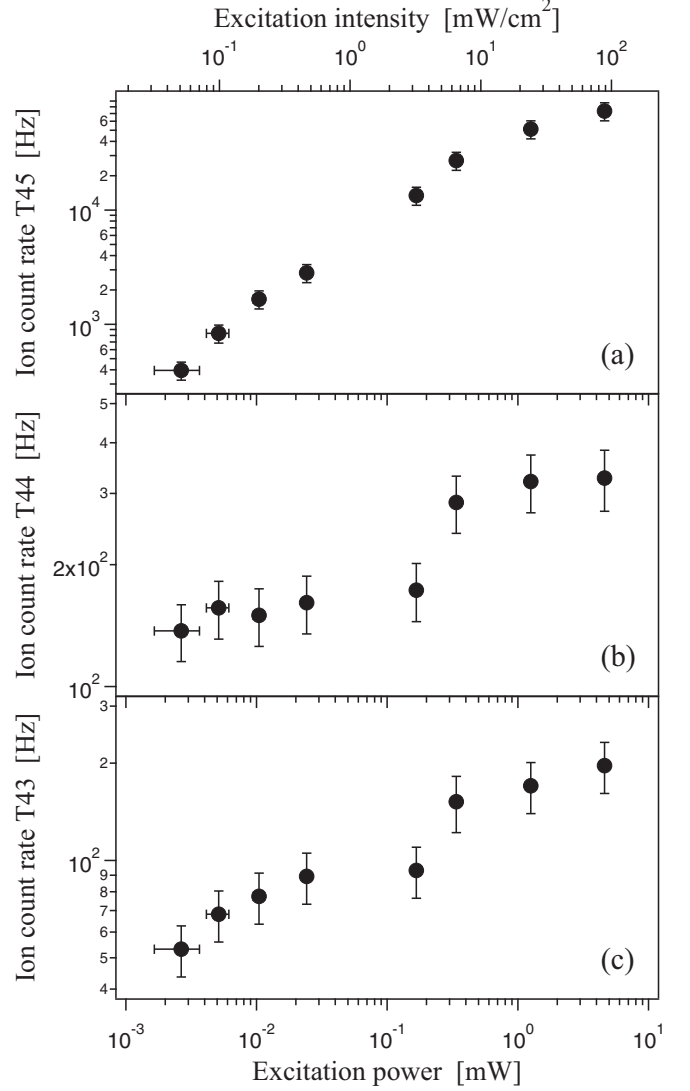


FIG. 4. Ion count rates for (a) T45, (b) T44, and (c) T43 transitions as a function of excitation power. For reference, the top axis reports the excitation intensity determined in the actual experimental conditions.

and ~ 0.2 mW, followed by a more marked increase at higher power. We will start the interpretation based on a conventional point of view of optical pumping before going into the details of more subtle effects described in the following sections.

A. Line-strength considerations

The increase in ion signal shown in Fig. 4 can be simply interpreted through optical pumping in a partially open two-level system. The Hamiltonian of laser-atom interaction can be written as

$$H_{ab}^{int} = \hbar \Omega_{ab}(t) \cos(\omega_L t), \quad (6)$$

where a and b label the atomic states ($a, b = 1, \dots, 43$; see Fig. 1) and $\Omega_{ab}(t)$ are the respective Rabi frequencies. Time dependence of the H_{ab}^{int} operator is given by (i) the laser electric field $E(t) = E_{exc} \cos(\omega_L t)$, accounting for fast oscillations at the frequency ω_L , and (ii) the spatial intensity profile of the pump laser field, $I(z) = I_{exc} \exp[-z^2/(w_z^{exc})^2]$. An atom

moving through the laser beam with the average flow velocity $\langle v \rangle$ will experience Gaussian switching of Rabi frequency [3]; the latter can be expressed through the reduced Rabi frequency Ω_{red} and dimensionless coupling coefficients C_{ab}^p as [20,23]

$$\Omega_{ab}(t) = \Omega_{red} C_{ab}^p \exp\left(-\frac{2t^2}{\tau_{tr,exc}^2}\right). \quad (7)$$

The C_{ab}^p coefficients for individual Zeeman $a \rightarrow b$ transitions driven by a polarized laser field ($p = 0, \pm 1$ for linear and right-/left-handed circular polarization, respectively) are related to the $3j$ symbols via the expression [23]

$$C_{ab}^p = \sqrt{\tilde{S}_{F_a F_b}} \begin{pmatrix} F_a & 1 & F_b \\ -m_a & p & m_b + p \end{pmatrix}. \quad (8)$$

The relative line strength $\tilde{S}_{F_a F_b}$ is connected to the line strength $S_{F_a F_b}$ and to the reduced dipole matrix element $D_{S,P} = (6 \cdot 2S_{1/2} ||D|| 6^2 P_{3/2})$ of the unresolved D_2 transition by

$$\tilde{S}_{F_a F_b} = \frac{S_{F_a F_b}}{D_{S,P}^2}. \quad (9)$$

The spontaneous decay rate $\Gamma_{F_a F_b}$ of individual HF transitions $F_a \rightarrow F_b$ is given by

$$\Gamma_{F_a F_b} = \frac{4\omega^3}{3\hbar c^3} \frac{1}{2F_b + 1} S_{F_a F_b}, \quad (10)$$

where ω is the angular frequency of the D_2 line. Figure 5 shows the $\tilde{S}_{F_a F_b}$ values together with the branching ratios $\Pi_{F_a F_b}$ for the HF transitions of interest. The reduced line strengths are normalized such that $\sum_{F_a, F_b} \tilde{S}_{F_a F_b} = 2I + 1 = 8$ [23], where $I = 7/2$ is the nuclear spin.

The Ω_{red} coupling strength is determined by the excitation-field amplitude E_{exc} via the $D_{S,P}$ reduced matrix element

$$\Omega_{red} = \frac{D_{S,P} E_{exc}}{\hbar}. \quad (11)$$

Its value can be readily determined from the experimental parameters, i.e., from the laser intensity $I_{exc} = W_{exc}/(\pi w_z^{exc} w_y^{exc})$, where W_{exc} is the power and w_z^{exc}, w_y^{exc} are the measured beam waists. According to [3,32],

$$\Omega_{red}^2 = I_{exc} \Gamma_e \frac{3\lambda^3 g_e}{4\pi^2 \hbar c}, \quad (12)$$

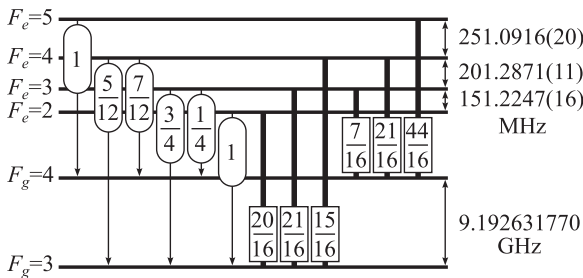


FIG. 5. Branching ratios Π_{F_a, F_b} (arrows with rounded frames) for $6^2S_{1/2} \rightarrow 6^2P_{3/2}$ HF transitions and relative line strengths $\tilde{S}_{F_a F_b}$ (thick lines with rectangular frames). HF frequency splittings are also shown [31].

where λ is the laser wavelength and $g_e = 4$ is the statistical weight of the $6^2P_{3/2}$ state. The Rabi frequencies of individual HF transitions are $\Omega_{F_a F_b} = \sqrt{\tilde{S}_{F_a F_b}} \Omega_{red}$.

At very small Ω_{red} , corresponding to regime (i) in Sec. II A, one expects the relative resonant peak intensities in the excitation spectra to correspond to the theoretical line strengths $\tilde{S}_{F_a F_b}$. In effect, the ratios of the ion counts of Fig. 4 measured for the T43, T44, and T45 transitions at weak excitation intensities match the relevant ratios of $\tilde{S}_{F_a=4, F_b=3,4,5}$. This is a typical case of regime (i) of optical pumping mentioned in Sec. II A, which is valid when $\Omega < \Omega_{cr}$.

B. Saturation power

Increasing laser power naturally leads to regime (ii) at Rabi frequencies $\Omega_{cr} < \Omega < \Omega_{sat}$, which is earmarked by significant population loss due to optical pumping and saturation of the observed signals. Each HF transition has a different value of Rabi frequency corresponding to the critical value; using Eq. (3), these are determined as $\sqrt{\tilde{S}_{F_a F_b}} \Omega_{cr}^{red} = \Omega_{cr}$. Equation (12), in turn, links Ω_{cr}^{red} to the respective experimental laser intensity I_{cr} .

Evaluation of the critical intensity for the considered transitions leads to values much smaller than the closed two-level saturation intensity, which is in the range of a few mW/cm² [31]. In particular, due to the very long transit time $\tau_{tr,exc}$ explored in our investigation, one obtains for the T44 and T43 transitions $I_{cr} = 1.9 \times 10^{-3}$ mW/cm² and $I_{cr} = 4.4 \times 10^{-3}$ mW/cm², respectively. In our experimental setup, they correspond to critical excitation laser powers $W_{cr} \approx 9.8 \times 10^{-5}$ mW and $W_{cr} \approx 2.3 \times 10^{-4}$ mW for T44 and T43, respectively. We note that excitation at such very small values of laser power has not been explored in our experiment due to the limitations imposed by the low particle density in the atomic beam and the relatively small laser-atom interaction volume. The ion count rates that could be achieved in this excitation limit were close to, or even below, the measurement uncertainty for the T44 and T43 transitions. Therefore the acquired measurements begin at laser power already large enough to induce optical pumping. The impact of optical pumping is obviously a function of laser power, as will be shown by the results of the numerical simulations presented in Sec. VI.

V. NUMERICAL SIMULATION SCHEME

A. Density-matrix master equation

The experimental interaction time $\tau_{tr,exc} \approx 180 \mu s$ is much larger than any radiative constants of the involved excited levels; hence optical pumping participates in determining the population dynamics even for the minimum excitation power used in the experiment. In order to properly take into account the accompanying nonlinear phenomena [18], we use the semiclassical formalism of optical Bloch equations [22]. Using the laser-atom interaction operator defined by Eqs. (6)–(10), the master equation for time evolution of the density-matrix elements ρ_{ab} can be written as [33]

$$\dot{\rho}_{ab} = -i\omega_{ab}\rho_{ab} - \frac{i}{\hbar} \sum_c (H_{ac}^{int} \rho_{cb} - \rho_{ac} H_{cb}^{int}) + I_{ab}, \quad (13)$$

where the terms l_{ab} describe the decay of excited-state populations ($a = b$) and of the off-diagonal coherences ($a \neq b$).

While the full dimension of Eq. (13) for the atomic system in Fig. 1 is $N \times N = 43^2 = 1849$, the use of linearly polarized light for the excitation reduces substantially the number of equations [20,34]. Equation (13) has a rotational symmetry around the pump laser polarization vector \vec{E}_{exc} , which is chosen as the quantization axis, resulting in conservation of the azimuthal (Zeeman) quantum number m [23]. Since initially ($t \rightarrow -\infty$) only the ground-state diagonal elements are nonzero, at all times only the matrix elements ρ_{ab} with $m_a = m_b$ are nonzero. A further simplification is possible due to the circumstance that only a single selected HF transition of the D_2 line is resonantly coupled with the excitation laser field; this allows us to disregard all off-diagonal terms ρ_{ab} involving the HF components of the $6^2P_{3/2}$ state ($a, b = 17, \dots, 43; F_a \neq F_b$) compared to the diagonal terms ρ_{bb} . Making use of the Hermitian properties of the density matrix and the rotating-wave approximation [22], whereby we replace the off-diagonal elements by the slowly varying variables $\sigma_{ab} = \rho_{ab} \exp(\pm i\omega_L t)$ in Eq. (13), we finally obtain the following 68 equations describing the evolution of the system [20,34]:

$$\text{for } a = 1, \dots, 7, \quad \frac{d\rho_{aa}}{dt} = \frac{g_e}{\tau_e} \sum_{p=-1}^1 \sum_{b=17}^{32} (C_{ab}^p)^2 \rho_{bb}, \quad (14)$$

for $a = 8, \dots, 16$,

$$\frac{d\rho_{aa}}{dt} = \sum_{b=17}^{43} \Omega_{ba} \text{Im}(\sigma_{ba}) + \frac{g_e}{\tau_e} \sum_{p=-1}^1 \sum_{b=17}^{43} (C_{ab}^p)^2 \rho_{bb}, \quad (15)$$

for $b = 17, \dots, 43$,

$$\frac{d\rho_{bb}}{dt} = \sum_{a=8}^{16} \Omega_{ab} \text{Im}(\sigma_{ab}) - \frac{1}{\tau_e} \rho_{bb} - r_{ion}(t) \rho_{bb}, \quad (16)$$

for $a = 8, \dots, 16, \quad b = 17, \dots, 43, \quad m_a = m_b$,

$$\frac{d\sigma_{ab}}{dt} = -\frac{i}{2} \Omega_{ba} (\rho_{bb} - \rho_{aa}) + i(\omega_{ab} - \omega_L) \sigma_{ab} - \frac{1}{2\tau_e} \rho_{ab}. \quad (17)$$

Equation (14) describes the increase of the $F_g = 3$ population due to spontaneous decay from the excited sublevels. In Eqs. (15) and (16) similar contributions due to the spontaneous decay enter along with laser coupling terms, both needed to describe the evolution of the $F_g = 4$ and $F_e = 3, 4, 5$ populations.

The third term in Eq. (16) takes into account the loss of population out of the hyperfine-level system due to photoionization by the probe laser field, the rate of which is given by [35,36]

$$r_{ion}(t) = \frac{\sigma_{ion} \lambda_{ion}}{hc} I_{ion}(t), \quad (18)$$

where $\lambda_{ion} = 405$ nm is the wavelength of the ionizing radiation, $\sigma_{ion} = 1.4 \times 10^{-17} \text{ cm}^2$ [37] is the photoionization

cross section, and $I_{ion}(t)$ is the intensity of the ionizing field. The time dependence of the latter is determined by the atom propagation through the Gaussian envelope of this laser field, $I_{ion}(t) = I_{0,ion} \exp(-4t^2/\tau_{tr,ion}^2)$. Under our experimental conditions the photoionization rate makes only a small fraction ($\leq 10^{-6}$) of the radiative transition rates; hence it can be considered a truly nonperturbing probe of the excited-state populations.

Finally, Eq. (17) describes the time dependence of the atomic coherences between the sublevels of ground and excited states.

Being computationally intensive, the numerical solutions of Eqs. (14)–(17) are carried out for a single atom traveling with the average beam velocity $\langle v \rangle$ through the center of the excitation laser beam. Initially, at $t \rightarrow -\infty$, the population is assumed to be equally distributed over the ground-state Zeeman levels, and the calculations are performed for the time interval between $-10\tau_{tr}$ and $+10\tau_{tr}$, whereby the zero of the time axis is chosen at the time of passage through the peak of the excitation laser intensity profile.

We remark that, in contrast to the treatment of the population dynamics in a simplified open level system developed in [3], here, we solve the complete system of relevant optical Bloch equations that naturally accounts for the time evolution of the nondiagonal density-matrix elements. Similar to [3], we expect the effect of coherences to be negligible at excitation below the saturation power, while the results for strong excitation indicate that laser-induced HF-level mixing becomes important. In solving the optical Bloch equations, we do not account for laser phase fluctuations, which are expected to play a negligible role in our experimental conditions.

B. The ionization signal

The measured ionization signal is proportional to the ionization probability P_{ion} per atom, which, in turn, depends on the computed excited-state occupations $\rho_{ee}(t)$:

$$P_{ion} = \int_{-\infty}^{+\infty} r_{ion}(t) \sum_{b=17}^{43} \rho_{bb}(t) dt. \quad (19)$$

The number of atoms dN_{at}^{exc} exposed to the probe laser field in the ionization volume between t and $t + dt$ is

$$dN_{at}^{exc}(t) = J_{at} \rho_{ee}(t) dt, \quad (20)$$

where J_{at} is the atom flux and ρ_{ee} is the total occupation of the excited $6^2P_{3/2}$ state. The number of ions generated per unit time via photoionization of those atoms between t and $t + dt$ is

$$dN_{ion}(t) = r_{ion} dN_{at}^{exc}(t) = J_{at} r_{ion}(t) \rho_{ee}(t) dt. \quad (21)$$

The ion count rate, i.e., the registered number of ions per unit time, is then

$$\begin{aligned} N_{ion}^{exp}(\delta, W_{exc}) &= \eta J_{at} \int_{-\infty}^{+\infty} r_{ion}(t) \rho_{ee}(t) dt \\ &= \eta J_{at} P_{ion}(F_g \rightarrow F_e, \delta, W_{exc}), \end{aligned} \quad (22)$$

where $\eta < 1$ is the efficiency of the ion-detection system. We explicitly indicate the dependence of the ionization rate on the chosen HF transition $F_g \rightarrow F_e$, the power W_{exc} of the

exciting laser field, and its detuning δ off from resonance with the chosen hyperfine transition. For a well-known collection efficiency η , Eq. (22) would enable a direct comparison between the calculated and experimentally measured ion count rates. Given the uncertainties in the absolute calibration of the ion-detection system, we rely on the excitation ratios for different HF levels $F_g \rightarrow F_e$, as these are exactly equal to the ratios of the respective simulated ionization probabilities:

$$\begin{aligned} R_{F'_g F'_e, F_g F_e} &= \frac{N_{ion}^{exp}(F'_g \rightarrow F'_e, \delta', W_{exc})}{N_{ion}^{exp}(F_g \rightarrow F_e, \delta, W_{exc})} \\ &= \frac{P_{ion}(F'_g \rightarrow F'_e, \delta', W_{exc})}{P_{ion}(F_g \rightarrow F_e, \delta, W_{exc})}. \end{aligned} \quad (23)$$

VI. NUMERICAL RESULTS AND DISCUSSION

A. Experiment and simulation

Figure 6 show the experimental (dots) and simulated (solid lines) ion signal ratios $R_{45,44}$ and $R_{44,43}$ in the case of resonant excitation ($\delta = 0$). For comparison, the dashed lines show the

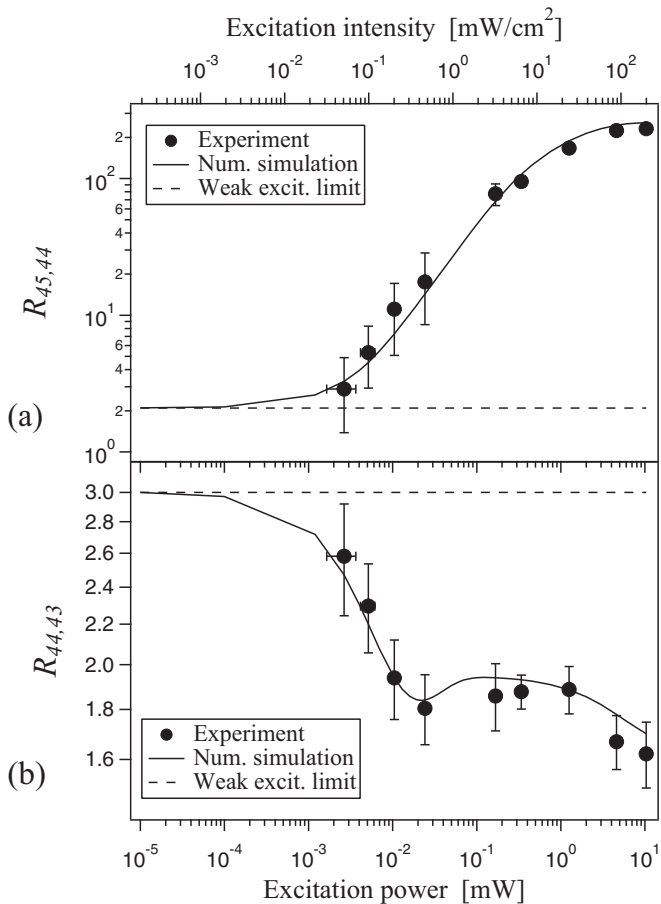


FIG. 6. Ratio (a) of the T45 and T44 ion signals and (b) of the T44 and T43 ion signals derived from data from Fig. 4 as a function of the excitation power. The dots represent the experimental data, while the lines are obtained from the simulation discussed in the text (solid line) and in the limit of weak excitation, i.e., from the $\tilde{S}_{F''F'}$ values (dashed lines). For reference, the top axis reports the excitation intensity determined in the actual experimental conditions.

corresponding values $R_{45,44} = 44/21$ and $R_{44,43} = 3$ obtained as ratios of line strengths $\tilde{S}_{F''F'}$ (see Fig. 5), valid in the linear excitation regime at weak excitation power, that is, in regime (i) mentioned in Sec. II A. The departure of the simulated results from the dashed line, occurring already at power values ($W_{exc} \sim 10^{-4}$ mW) below the experimentally explored range, is a clear signature of the occurrence of the critical values reported in Sec. IV B.

The first immediate observation from Fig. 6(a) is the hundredfold growth of the ratio $R_{45,44}$ as the excitation power increases from $\sim 10^{-3}$ to ~ 1 mW (the corresponding excitation intensity, reported on the top axis, ranges from ~ 0.02 to ~ 20 mW/cm²). This is a consequence of the fast growth in the ion yield upon T45 excitation, which is not compensated by an equivalent increase upon excitation of T44. At the same time, the ratio $R_{44,43}$ [Fig. 6(b)] exhibits a minimum for an excitation power around $20 \mu\text{W}$, corresponding to an intensity around 0.4 mW/cm². That minimum value can be estimated from the ratio of the averaged excited-state occupations at saturation given by Eq. (5): using the data from Fig. 5, the result is $(1 - \Pi_{43})/(1 - \Pi_{44}) = 9/5$, in very good agreement with the measurement.

A thorough analysis including a comparison between experimental and numerical results and accounting for hyperfine and Zeeman pumping, which both play a substantial role under the conditions of our experiment, is provided in the following sections.

B. $F_g = 4 \rightarrow F_e = 5$ excitation

Figure 7 shows the simulated evolution of the populations of hyperfine levels during the passage of atoms through the excitation laser field for small [Figs. 7(a1), 7(b1), and 7(c1)] and large [Figs. 7(a2), 7(b2), and 7(c2)] excitation powers, expected to correspond to regime (ii) and regime (iii) in Sec. II A, respectively. The zero of the horizontal axis corresponds to the peak of the intensity profile for the excitation laser. At low excitation power the population of the $F_e = 5$ level closely follows the Gaussian profile of the excitation laser beam, with an expected (and negligible) leak of population to the $F_e = 4$ level, while the population of level $F_g = 3$, which acts as the population “sink,” is not significantly modified.

This situation changes dramatically at high excitation power because T45 can no longer be considered a “cycling” transition. The off-resonant laser coupling to other excited HF levels, equivalent to state mixing [38], leads to a substantial increase in the population of levels $F_e = 3, 4$. Even if this population transfer is small, the long interaction time ensures strong optical pumping to the sink level $F_g = 3$. A further interesting detail in Fig. 7(a2) is the appearance of a small plateau in the population of $F_e = 5$ at $t \approx 200 \mu\text{s}$, occurring when the population of $F_g = 4$ is strongly depleted as in Fig. 7(c2). Understanding this observation requires closer inspection of the population dynamics of $F_g = 4$ and $F_e = 5$ during the laser pulse. At $t \approx -300 \mu\text{s}$ the intensity of the excitation field is so low that the atoms are excited almost exclusively to $F_e = 5$, which is accompanied by a corresponding decrease of the population in $F_g = 4$. Once the atoms reach the center of the laser beam, the laser intensity becomes sufficiently high to mix the HF levels, whereby the

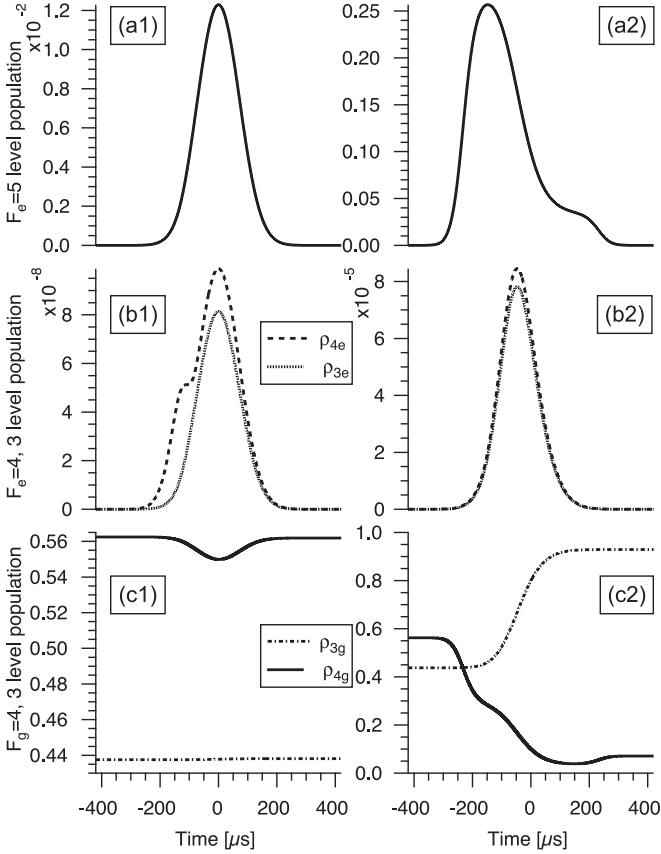


FIG. 7. Evolution of the populations in the hyperfine sublevels (a1), (a2) $F_e = 5$, (b1), (b2) $F_e = 3, 4$, and (c1), (c2) $F_g = 3, 4$ during the atom propagation across the excitation laser beam resonant with the T45 transition. Laser power is $W_{exc} = 3 \mu\text{W}$ (corresponding to $I_{exc} = 58 \mu\text{W}/\text{cm}^2$) in (a1), (b1), and (c1) and $W_{exc} = 10 \text{ mW}$ (corresponding to $I_{exc} = 190 \text{ mW}/\text{cm}^2$) in (a2), (b2), and (c2).

adiabatic state consisting of the laser-coupled levels $F_g = 4$ and $F_e = 5$ starts sharing population with the $F_e = 3, 4$ levels. The population of the latter two opens a spontaneous decay leak to $F_g = 3$, and the optical pumping sets in. Once the atoms have passed the peak laser intensity, the effect of state mixing weakens and ultimately vanishes; at this point all atoms remaining in the $F_g = 4$ level are again excited only to the $F_e = 5$ level, resulting in the additional small plateau in the population of $F_e = 5$.

The strong population sharing between the adiabatic state composed of $F_g = 4$, $F_e = 5$ and the levels $F_e = 3, 4$ modifies the T45 transition to semiopen, such that the effective branching ratio is $\Pi_{45}^{eff}(t) < 1$. Equation (5) shows that our measured signal, which depends on $\bar{n}_e^{(sat)}$, is very sensitive to variations of the effective branching ratio near its initial value $\Pi_{45}^{eff}(t = -\infty) = 1$.

We have linked the evolution of the T45 excitation to the so-called bright-resonance phenomenon introduced by Alnis and Auzinsh [24], which in our case strongly affects the Π_{45}^{eff} value. Figure 8 shows a simplified level diagram illustrating the key features of the population redistribution within the $|F_g = 4, m_g\rangle$ Zeeman sublevels. The diagram is restricted to the sublevels around $m = 0$, where the linearly polarized

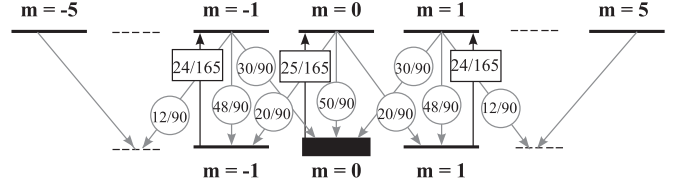


FIG. 8. Schematic illustration of bright-resonance formation within the Zeeman multilevel system involved in the T45 transition, showing partial spontaneous decay rates Γ_m^p (circular frames), in units of Γ_e , and absorption rates Λ_m (square frames), in arbitrary units. The thick line denotes the ground state contributing to the bright resonance. For the sake of clarity, details of transitions and relevant rates are reported only for a selected choice of states ($m = 0, \pm 1$ for both excited and ground states).

light produces a population alignment through the optical pumping. The decay rates Γ_m^p , proportional to the square of the $3j$ symbols of Eq. (8) and reported in circle frames in the figure, indicate a noticeably slower leak of population from the pair $m_e = m_g = 0$ compared to the other m -state pairs. Consequently, at equilibrium the largest population is cycled within those “bright” magnetic sublevels at the expense of the population loss from other m -state pairs. In our case, this phenomenon has an interesting effect at strong laser coupling. In the presence of state mixing, because the vertical T44 transition from $m_g = 0$ is forbidden, the bright-state formation substantially reduces the efficiency of the leak channel of decay $F_e = 4 \rightarrow F_g = 3$ opened by the mixing. Such depletion inhibition, in turn, leads to an increase in the effective T45 branching ratio Π_{45}^{eff} and therefore contributes to the ion signal increase.

C. $F_g = 4 \rightarrow F_e = 3$ and $F_g = 4 \rightarrow F_e = 4$ excitations

Figure 9 shows the simulated evolution of populations upon excitation of the T44 transition. A strong depletion of the $F_g = 4$ level takes place already in the weak-excitation regime [Fig. 9(c1)], corresponding to regime (ii) in Sec. II A, which agrees with the low critical excitation power for this transition (see Sec. IV B). This depletion is caused by population loss to $F_g = 3$ via spontaneous decay from $F_e = 4$. In addition, as pointed out previously, the level $|F_g = 4, m = 0\rangle$ acts as a dark Zeeman sublevel trapping the population [see Fig. 2(a)]. The solid line in Fig. 10, showing the simulated evolution of the $|F_g = 4, m = 0\rangle$ population at weak excitation laser power [regime (ii)], indicates that accumulation of population in this level takes place during the propagation of atoms across the laser field.

In the strong excitation regime i.e., well within regime (iii), the $F_e = 4$ population shows an auxiliary peak at $t \approx -150 \mu\text{s}$ [see Fig. 9(b2)]. This phenomenon is explained by the laser-field-induced mixing of HF levels combined with Zeeman optical pumping. The dashed line in Fig. 10 shows that the population of $|F_g = 4, m_g = 0\rangle$ increases only for $t \lesssim -200 \mu\text{s}$, when the atoms are in the wing of the laser intensity profile. At the laser beam center, the increased coupling strength induces transitions to the levels $|F_e = 3, m_e = 0\rangle$ and $|F_e = 5, m_e = 0\rangle$, which pump the population out of $|F_g = 4, m_g = 0\rangle$. Since atoms in $|F_e = 3, m_e = 0\rangle$ and $|F_e = 5, m_e = 0\rangle$ can decay to

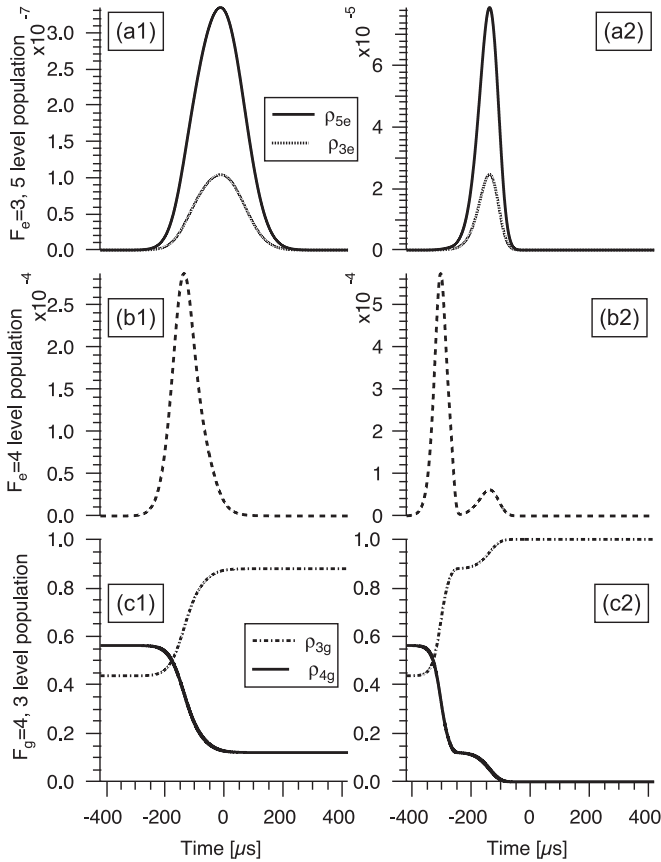


FIG. 9. Evolution of the populations in the hyperfine sublevels (a1), (a2) $F_e = 3, 5$, (b1), (b2) $F_e = 4$, and (c1), (c2) $F_g = 3$ during the atom propagation across the excitation laser beam resonant with the T44 transition. Laser power is $W_{exc} = 3 \mu\text{W}$ (corresponding to $I_{exc} = 58 \mu\text{W}/\text{cm}^2$) for (a1), (b1), and (c1) and $W_{exc} = 10 \text{ mW}$ (corresponding to $I_{exc} = 190 \text{ mW}/\text{cm}^2$) for (a2), (b2), and (c2).

$F_g = 4$ with $m_g \neq 0$, they can be reexcited to $F_e = 4$ in the next excitation cycle, leading to the small increase in the $F_e = 4$ population at $t \approx -150 \mu\text{s}$ shown in Fig. 9(b2). Finally, the

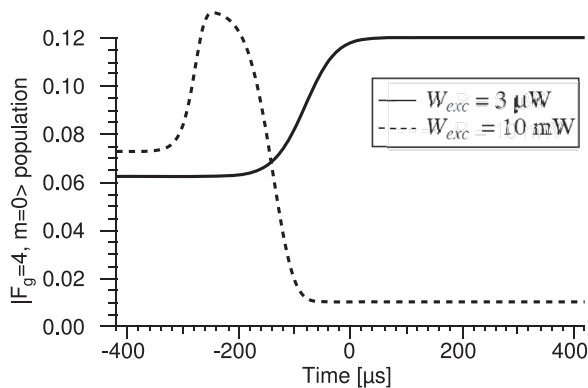


FIG. 10. Evolution of the $|F_g = 4, m = 0\rangle$ state population during the atom propagation across the excitation laser beam resonant with the T44 transition. The quite different behaviors for low and high radiation powers, expected to correspond to regimes (ii) and (iii), are shown with solid and dashed lines, respectively.

$F_g = 4$ population is almost entirely pumped into the $F_g = 3$ level, which is not coupled to excited F_e levels.

Similar to the T45 case, the retrieval of population from $|F_g = 4, m_g = 0\rangle$ can be interpreted in terms of the increase in the effective branching ratio $\Pi_{44}^{eff} > \Pi_{44}(t = -\infty)$. According to Eq. (5), that also increases the ion count rate, as observed in the experimental results of Fig. 4(b). We note that, for T44 such an increase is not as dramatic as in the case of T45 because the $\Pi_{44}(t = -\infty)$ value is well below unity (see Fig. 5). This different behavior explains the rapid growth of the ion signal ratio $R_{45,44}$ shown in Fig. 6(a).

The evolution of populations upon T43 excitation is essentially similar to that observed in the T44 case, with the role of the dark states being played here by the outermost Zeeman sublevels $|F_g = 4, m_g = \pm 4\rangle$ [see Fig. 2(b)]. We will not go into a detailed description of the involved processes, and we will focus on only the interpretation of the $R_{44,43}$ behavior [see Fig. 6(b)]. As shown in Fig. 7, at small excitation power ($W_{exc} \lesssim 10^{-2} \text{ mW}$, i.e., in regime (ii) in Sec. II A, the population of $F_e = 4$ decreases more rapidly than that of $F_e = 3$ with increasing W_{exc} because optical pumping in the case of T44 is more efficient than for T43 (see [3] for a more detailed discussion). The rebound in $R_{44,43}$ at $W_{exc} \sim 0.1 \text{ mW}$, corresponding to $I_{exc} \sim 2 \text{ mW}/\text{cm}^2$, is related to the onset of excitation from the dark Zeeman sublevel $F_g = 4, m_g = 0$ enabled by state mixing upon T44 excitation. The further decrease in $R_{44,43}$ at $W_{exc} > 1 \text{ mW}$, i.e., for $I_{exc} \gtrsim 20 \text{ mW}/\text{cm}^2$, is explained by extraction of population from the dark states $F_g = 4, m_g = \pm 4$ upon T43 excitation, where in this case two dark Zeeman sublevels donate their population and remarkable state mixing occurs due to the circumstance that the transition strength is smaller for T43 than for T44.

D. Ion production control

We stress that the measured ion counts depend in a nontrivial way on the excitation laser power. As a matter of fact, an increase in the excitation power from $3 \mu\text{W}$ to 10 mW increases the peak value of the $F_e = 5$ population by around 20 times [see Figs. 7(a1) and 7(a2)]. Under the same conditions, the peak value of the $F_e = 4$ level population increases by around a factor of 2 [see Figs. 9(b1) and 9(b2)]. This would lead to accounting for a growth of the $R_{45,44}$ ratio by a factor $\sim 20/2 = 10$.

The measured $R_{45,44}$ exhibits instead a hundredfold growth for the same excitation power increase, which is a signature of the role played by the excitation laser through the combined effect of light-induced state mixing and optical pumping. However, the measured value depends also on the spatial overlap of the excitation and ionization lasers within the region of atom-laser interaction. The overlap control achieved in the present experiment is not at the required accuracy level to allow for a detailed characterization. In future applications, the overlap will be controlled by carefully acting on the geometrical features of the excitation and photoionization laser beams. This could open interesting perspectives for spatially selective dynamical preparation and also for ultrasensitive detection of populations in selected HF levels.

VII. CONCLUSIONS

We have studied the effects of population dynamics upon resonant excitation of the Cs D_2 line in a beam of slow and cold atoms, enabling the experimental achievement of very long atom-light interaction times (around 180 μ s). By probing the excited-state population through photoionization, nonperturbing analysis of the excited-state population has been attained together with an excellent sensitivity that allows us to investigate the population dynamics over a wide range of pumping laser power. If the excitation intensity is sufficiently large, the atoms will consecutively experience excitation regimes (i)–(iii) defined in Sec. II A during their passage through the laser beam. Owing to adiabatic switching of laser-atom interaction, such passage gives rise to subsequent stages of optical pumping: the linear stage at weak laser field in the wings of the Gaussian laser intensity profile (stage I); the critical to saturation stage, when coupling between the ground and excited levels leads to remarkable population depletion in a semiopen level scheme (stage II); the intermediate stage, when population redistribution over HF Zeeman sublevels is accompanied by accumulation of the population in bright and dark magnetic sublevels of the ground state (stage III); and the nonlinear stage occurring at peak laser intensities, which features laser-induced mixing of HF levels and depletion of population from the dark magnetic sublevels (stage IV).

In contrast to an earlier study [3], which dealt with optical pumping in the weak excitation limit covering stages I–III, emphasis has been given here to the nonlinear stage IV, made accessible thanks to the specific experimental configuration. Within this context, we have shown that the presence of bright and dark Zeeman sublevels leads to variations in the effective branching coefficients Π^{eff} , and these variations have non-

trivial effects on the dependence of excited-state populations on the laser power. The population can accumulate in dark states in stage III, which leads to a decreased Π^{eff} , while the retrieval of population from the dark states due to laser-induced mixing in stage IV increases Π^{eff} . Moreover, the mechanism of bright-resonance formation can lead to a decreased Π^{eff} , while the optical pumping is partially blocked due to specific selection rules, producing an increased Π^{eff} . We have demonstrated how the interplay between the various factors affecting the population dynamics can lead to significant and intuitively unpredictable variations in HF-level populations. They become particularly pronounced when using laser-manipulated atoms even at relatively weak laser intensities, owing to the explored long atom-light interaction-time regimes.

ACKNOWLEDGMENTS

N.P., G.S., A.F., I.G., D.C., M.V., and F.F. acknowledge gratefully the support of the European Commission Seventh Framework Programme under Grant No. 251391 MC-IAPP “COLD BEAMS.” This collaborative work was supported also by the European Commission Seventh Framework Programme IRSES project COLIMA and the Centre of Excellence FOTONIKA-LV (European Commission Seventh Framework Programme project REGPOT-CT-2011-285912-FOTONIKA). N.B. acknowledges the support from Government of the Russian Federation Grant No. 074-U01, and M.B. and A.E. acknowledge the support from U.S. Office of Naval Research Grant No. N00014-12-1-0514. We thank Professor M. Auzinsh for helpful discussions on the bright-resonance phenomena and N. Puccini and E. Andreoni for their assistance with the experiment.

-
- [1] W. Happer, *Rev. Mod. Phys.* **44**, 169 (1972).
 - [2] K. B. Im, H. Y. Jung, C. H. Oh, S. H. Song, P. S. Kim, and H. S. Lee, *Phys. Rev. A* **63**, 034501 (2001).
 - [3] I. Sydoryk, N. N. Bezuglov, I. I. Beterov, K. Miculis, E. Saks, A. Janovs, P. Spels, and A. Ekers, *Phys. Rev. A* **77**, 042511 (2008).
 - [4] J. Sagle, R. K. Namiotka, and J. Huennekens, *J. Phys. B* **29**, 2629 (1996).
 - [5] W. K. Hensinger, A. G. Truscott, H. Rubinsztein-Dunlop, and N. R. Heckenberg, *Opt. Quantum Electron.* **31**, 391 (1999).
 - [6] D. A. Smith and I. G. Hughes, *Am. J. Phys.* **72**, 631 (2004).
 - [7] G. Avila, V. Giordano, V. Candelier, E. de Clercq, G. Theobald, and P. Cerez, *Phys. Rev. A* **36**, 3719 (1987).
 - [8] L. C. Balling, in *Advances in Quantum Electronics*, edited by D. W. Goodwin (Academic Press, New York, 1975), Vol. 3, pp. 1–167.
 - [9] J. E. M. Haverkort, H. G. C. Werij, and J. P. Woerdman, *Phys. Rev. A* **38**, 4054 (1988).
 - [10] B. J. Claessens, S. B. van der Geer, G. Taban, E. J. D. Vredendregt, and O. J. Luiten, *Phys. Rev. Lett.* **95**, 164801 (2005).
 - [11] J. L. Hanssen, J. J. McClelland, E. A. Dakin, and M. Jacka, *Phys. Rev. A* **74**, 063416 (2006).
 - [12] J. L. Hanssen, S. B. Hill, J. Orloff, and J. J. McClelland, *Nano Lett.* **8**, 2844 (2008).
 - [13] M. P. Reijnders, P. A. van Kruisbergen, G. Taban, S. B. van der Geer, P. H. A. Mutsaers, E. J. D. Vredendregt, and O. J. Luiten, *Phys. Rev. Lett.* **102**, 034802 (2009).
 - [14] L. Kime, A. Fioretti, Y. Bruneau, N. Porfido, F. Fusco, M. Viteau, G. Khalili, N. Santic, A. Gloter, B. Rasser, P. Sudraud, P. Pillet, and D. Comparat, *Phys. Rev. A* **88**, 033424 (2013).
 - [15] K. A. Twedt, L. Chen, and J. J. McClelland, *Ultramicroscopy* **142**, 24 (2014).
 - [16] S. H. W. Wouters, G. ten Haaf, R. P. M. J. W. Notermans, N. Debernardi, P. H. A. Mutsaers, O. J. Luiten, and E. J. D. Vredendregt, *Phys. Rev. A* **90**, 063817 (2014).
 - [17] D. H. Yang and Y. Q. Wang, *Opt. Commun.* **74**, 54 (1989).
 - [18] T. J. O’Kane, R. E. Scholten, P. M. Farrell, and M. R. Walkiewicz, *Phys. Rev. A* **59**, 4485 (1999).
 - [19] G. Moon and H.-R. Noh, *Opt. Commun.* **281**, 294 (2008).
 - [20] L. P. Maguire, R. M. W. van Bijnen, E. Mese, and R. E. Scholten, *J. Phys. B* **39**, 2709 (2006).
 - [21] C. Cohen-Tannoudji, *Rev. Mod. Phys.* **70**, 707 (1998).
 - [22] Bruce W. Shore, *Manipulating Quantum Structures Using Laser Pulses* (Cambridge University Press, Cambridge, 2011).

- [23] I. I. Sobel'man, *Atomic Spectra and Radiative Transitions* (Springer, Berlin, 1999).
- [24] J. Alnis and M. Auzinsh, *J. Phys. B* **34**, 3889 (2001).
- [25] F. Tantussi, V. Mangasuli, N. Porfido, F. Prescimone, F. Fuso, E. Arimondo, and M. Allegrini, *Appl. Surf. Sci.* **255**, 9665 (2009).
- [26] F. Tantussi, A. Camposeo, M. Alderighi, N. Puccini, E. Andreoni, M. Allegrini, and E. Arimondo, *Mater. Sci. Eng. C* **27**, 1418 (2007).
- [27] A. Camposeo, F. Cervelli, A. Piombini, F. Tantussi, F. Fuso, M. Allegrini, and E. Arimondo, *Mater. Sci. Eng. C* **23**, 217 (2003).
- [28] H. R. Noh and W. Jhe, *Phys. Rep.* **372**, 269 (2003).
- [29] J. J. Arlt, O. Maragò, S. Webster, S. Hopkins, and C. J. Foot, *Opt. Commun.* **157**, 303 (1998).
- [30] A. Camposeo, A. Piombini, F. Cervelli, F. Tantussi, F. Fuso, and E. Arimondo, *Opt. Commun.* **200**, 231 (2001).
- [31] D. A. Steck, Cesium D Line Data, <http://steck.us/alkalidata>
- [32] P. M. Farrell and W. R. MacGillivray, *J. Phys. A* **28**, 209 (1995).
- [33] K. Blum, *Density Matrix: Theory and Applications* (Plenum, New York and London, 1996).
- [34] J. J. McClelland and M. H. Kelley, *Phys. Rev. A* **31**, 3704 (1985).
- [35] O. Maragò, D. Ciampini, F. Fuso, E. Arimondo, C. Gabbanini, and S. T. Manson, *Phys. Rev. A* **57**, R4110 (1998).
- [36] B. M. Patterson, T. Takekoshi, and R. J. Knize, *Phys. Rev. A* **59**, 2508 (1999).
- [37] K. J. Nygaard, R. E. Hebner, J. D. Jones, and R. Corbin, *Phys. Rev. A* **12**, 1440 (1975).
- [38] This off-resonant excitation of the HF levels plays an important role in the operation of the magneto-optical traps. Within a dressed-atom description, the excitation within a V atomic scheme leads to a mixing of the excited-state wave functions.